Journal of Power Sources 195 (2010) 5534–5542

Contents lists available at ScienceDirect

Journal of Power Sources

journal homepage: www.elsevier.com/locate/jpowsour

A possible solution to the mechanical degradation of Ni–yttria stabilized zirconia anode-supported solid oxide fuel cells due to redox cycling

V. Vedasri, J.L. Young, V.I. Birss*

Department of Chemistry, University of Calgary, 25000 University Drive NW, Calgary, Alberta T2N 1N4, Canada

ARTICLE INFO

Article history:
Received 22 December 2009
Received in revised form 12 March 2010
Accepted 12 March 2010
Available online 19 March 2010

Keywords:
Ni–YSZ anodes
Redox cycling
Ni oxidation
Solid oxide fuel cells
Cell cool-down
Electrolyte cracking

ABSTRACT

The viability of cooling a solid oxide fuel cell (SOFC) during air exposure is investigated as a possible solution to the mechanical damage caused by inadvertent 'redox cycling' (cyclic exposure to air and then to H_2) of Ni-based anode-supported cells at high temperatures. In order to prevent electrolyte (and cell) cracking, it is shown that cooling the anode-supported Ni–YSZ samples during air exposure from 800 °C to <600 °C at rates >3 °C min^{-1} significantly slows down the oxidation of Ni. This, in turn, minimizes the volume expansion due to NiO formation. Cell cooling rates of <3 °C min^{-1} result in the cracking of the thin electrolyte layer, as sufficient time is then available for substantial NiO formation. It is also shown that partial oxidation during cool-down results in more extensive Ni oxidation in the outer regions of the anode layer compared to regions closer to the electrolyte. For the anode-supported cells investigated here, the electrolyte resists cracking when the nearby Ni particles (within 10–20 μm of the electrolyte) are prevented from oxidizing to an extent of more than 65%.

1. Introduction

Solid oxide fuel cells (SOFCs) are electrochemical devices that provide numerous advantages over other energy conversion systems, such as reliability, scalability, fuel flexibility, very low emissions of NO_x, SO_x, and particulates, and efficient conversion of fuels into electrical energy and high quality waste heat. The operating temperatures of SOFCs range between 600 and 1000 °C, depending on the materials used in cell construction and the design. These high temperatures result in rapid electrode reaction kinetics, while also allowing the direct use of hydrocarbon as fuels (components that are poisons in low temperature fuel cells, such as CO, are readily oxidized and removed in SOFCs) [1].

The most commonly employed material for anodes in SOFCs is a Ni–YSZ (yttria stabilized zirconia) cermet. These composites are widely used due to their low cost and ease of fabrication, a low charge transfer resistance (excellent electrocatalytic activity) for hydrogen oxidation [2], good physical stability (well-matched thermal expansion coefficients of Ni and YSZ, i.e., a value of 12.5×10^{-6} cm cm^{-1} K^{-1} for a Ni–YSZ 50:50 wt ratio cermet vs. 10.8×10^{-6} cm cm^{-1} K^{-1} for YSZ alone [3]) and good chemical stability in manufacturing and in reducing atmospheres. In conventional electrolyte-supported SOFCs, YSZ layers are relatively thick (0.1–0.5 mm) [4] and the ohmic resistance is therefore high. This resistance can only be overcome by using higher operating temperatures (900–1000 °C) [5]. Thus, recent efforts have been focused on the development of electrode-supported cells containing a thin electrolyte layer (5–20 μm thick YSZ). Anode-supported cells have been favored, due to their low ohmic resistance and manufacturability, and this has resulted in lower SOFC operating temperatures (<800 °C) [6–8].

Although anode-supported cells have advantages over cathode- and electrolyte-supported cells, they are more susceptible to mechanical damage caused by inadvertent oxidation by air, termed "redox cycling". The consequence of air break-in on the anode side by possible occurrences such as system shutdown, fuel supply interruption, and seal leakage, all at high temperatures, is the oxidation of the metallic Ni particles to form NiO. This leads to a volume expansion of >60% that generates stresses within the anode support layer (ASL), the active anode layer (the anode functional layer, AFL), and also in the electrolyte [8]. Cassidy et al. [9] observed significant cracking of the electrolyte after one redox cycle of a Ni–YSZ anode-supported cell. Other studies have shown that redox cycling of Ni–YSZ anodes can cause loss of electrochemical performance [10], with an increasing polarization resistance attributed to the development of cracks within the bulk sample, thus interrupting current pathways and decreasing the active triple phase boundary length [11].

Maintenance solutions to the redox cycling problem currently include purging with N_2 gas, but this is not always feasible in remote locations [12]. System solutions to the redox cycling problem are generally very costly due to the high operating temperature

* Corresponding author. Tel.: +1 403 220 6432; fax: +1 403 289 9488.
E-mail address: birss@ucalgary.ca (V.I. Birss).

0378-7753/$ – see front matter © 2010 Elsevier B.V. All rights reserved.
doi:10.1016/j.jpowsour.2010.03.043

of SOFCs. Although new anode materials, such as (La, Sr)(Cr,Mn)O_3 perovskites [13,14], are being investigated, no Ni-free anodes have yet been proven to be adequate in terms of performance or long-term operation. It has also been observed that the propensity for cracking can be decreased by lowering the Ni content in the Ni–YSZ anode layers and also by decreasing the cell temperature [15]. It is known [16–18] that the kinetics of Ni oxidation are temperature-activated and time-dependant, slowing down substantially at temperatures below 550–600 °C. Liu et al. [16], for example, demonstrated that, for a Ni–YSZ anode oxidized at 500 °C, the ohmic resistance does not change for at least 450 min, indicating that the oxidation rate is so slow at this temperature that the metallic Ni electronic conduction network is not destroyed. Attempts have also been made to restrict air flow into the anode by using an anode containing an oxidation barrier layer [19] to protect the Ni–YSZ anode from extensive oxidation.

In the present work, an economical and easily implemented method to minimize the deleterious effect of redox cycling of anode-supported Ni–YSZ cells is proposed. Using conventional Ni–YSZ microstructures, it is shown for the first time that anode-supported cells can be cooled down during air exposure at a rate that both minimizes the amount of Ni oxidized and avoids cracking due to thermal shock. Cooling rates of 3 °C min^{-1} (or higher) during oxygen exposure are found to be optimal. Once the temperature has been lowered to 550–600 °C, further Ni oxidation is minimal, as the kinetics of Ni oxidation are then very slow [20]. Importantly, a gradient in the NiO content of the anode support layer has been shown to exist, with the outer regions being significantly more oxidized than are the Ni particles located closer to the electrolyte. Therefore, cells that are over 75% oxidized overall are still less than 65% oxidized near the electrolyte and hence the local stresses are small enough such that no electrolyte cracking or other forms of degradation are observed.

2. Experimental methods

2.1. Sample preparation

The Ni–YSZ anode support layer (ASL) was constructed by tape casting (1.1 mm thick), followed by screen printing, successively, a thin (10 μm) AFL and a thin (10 μm) YSZ electrolyte layer onto the ASL, followed by firing in air at 1350 °C for 2 h (Fig. 1). The diameter of the samples after sintering was 1.6 cm. As no electrochemical performance measurements were carried out in this work, a cathode layer was not deposited on the anode-supported YSZ surface.

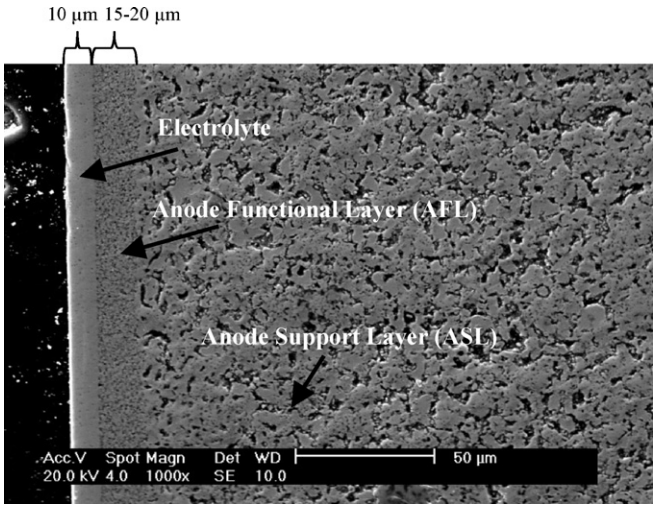

Fig. 1. Cross-sectional BSE-SEM view of anode-supported Ni–YSZ half-cell (without a cathode attached), showing the anode support layer on right part of image (coarse microstructure), then the anode functional layer (fine microstructure), and then the electrolyte layer on left side of image.

A cross-sectional SEM image of a typical Ni–YSZ support layer, attached to a thin YSZ electrolyte layer and reduced in 5% H_2–He at 800 °C, is shown in Fig. 1. The dense layer on the left-hand side of the image is the 10 μm thick YSZ electrolyte, the relatively thin anode functional layer (AFL, 10 μm) is seen just to its right, and the anode support layer (ASL, 1 mm thick) is shown as the thickest layer to the right of the AFL in Fig. 1.

2.2. Redox cycling protocols

Mass changes during isothermal and non-isothermal redox cycling of a Ni–YSZ composite anode half-cell were tracked using a Setaram TAG 16 dual chamber Thermogravimetric Analyzer. Small pieces of the anode half-cell (200 ± 50 mg) were placed into a shallow 100 μL Pt crucible and then heated in the 20% O_2–He carrier gas to the testing temperature (800 °C) at 5 °C min^{-1}. The flow was then switched to N_2 for a 10 min purge and then to 10% H_2–He carrier gas to achieve NiO reduction.

In the redox cycling experiments, when the H_2 was turned off, O_2 was introduced, with 5 min of N_2 flow between each gas, as illustrated in Fig. 2 (isothermal redox cycling, maintaining the temperature at 800 °C) and Fig. 3 (non-isothermal redox cycling, involving periodic sample cooling to 250 °C and re-heating). These

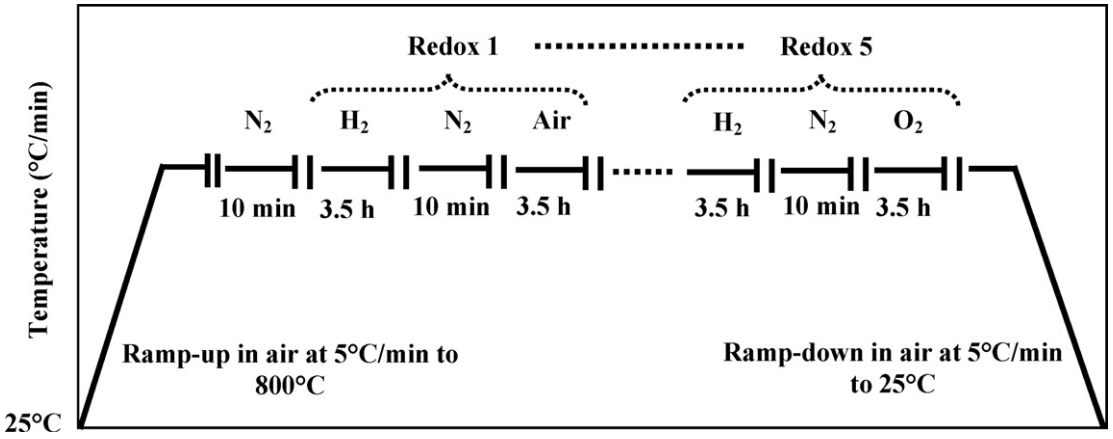

Fig. 2. Temperature and gas atmosphere profile used for redox cycling of Ni–YSZ/YSZ samples (Fig. 1) at 800 °C. Total number of $H_2/N_2/O_2$ cycles was typically 5. The multiple small parallel lines indicate change of gas atmosphere during redox cycling.

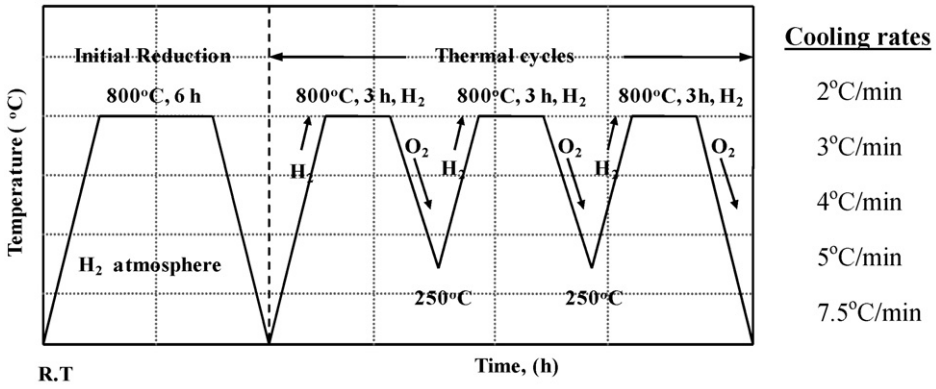

Fig. 3. Temperature and gas atmosphere profile used during redox cycling of Ni–YSZ/YSZ samples (Fig. 1) at 7.5 °C min^{-1} heating rate in H_2 and at various cell cool-down rates, all from 800 °C, during air exposure. Total number of $H_2/N_2/O_2$ cycles was typically 9.

cycles were repeated nine times to ensure that any cumulative damage from sintering would also be captured. In the isothermal redox cycling experiments, the samples were cooled to room temperature in each cycle, while in the non-isothermal redox cycling experiments, the samples were cooled down to 250 °C at a range of cooling rates, from 2 to 7.5 °C min^{-1}, in each cycle. After eight cycles, the samples were cooled to room temperature for further analysis.

2.3. Characterization methods

Scanning electron microscopy (SEM) analysis was performed using a Philips FEI Environmental Scanning Electron Microscope in vacuum mode (Microscopy and Imaging Facility, University of Calgary), also equipped with energy dispersive X-ray spectroscopy (EDX) capabilities. The Ni–YSZ anode-supported samples were then gold-coated prior to examination to avoid charging effects. The thickness of NiO film on Ni particles located 0.95 mm into Ni–YSZ anode support layer was determined from the cross-sectional SEM images using ImageJ Software.

The thin YSZ electrolyte layer was also examined optically (top-down), using a *Microstar American Optical* microscope, after multiple redox cycles to detect any cracks that had formed. Typical magnifications of 40–60 times were employed for the optical analyses.

3. Results and discussion

3.1. Cell microstructure

Fig. 1 shows that the thin AFL (57 wt% NiO) contains fine, well-distributed particles (initially ~0.5 μm in diameter) with a ~15% porosity after manufacturing and 30–5% porosity after NiO is reduced to Ni. In comparison, the ASL (also 57 wt% NiO) was fabricated using NiO and YSZ powders of ~1 μm average particle size and thus it has a higher porosity (~22% after manufacturing and ~38% after NiO reduction) than the AFL. It has been shown [21] that, after sintering, the NiO and YSZ particle sizes (initially ~1 μm) increase to 2–5 and 1–3 μm, respectively, and thus the reduced Ni particles are 1.5–3.7 μm in diameter [21]. With further re-oxidation, the NiO particles can become as large as 2.5–6 μm in size [21].

The differences in the microstructure of the AFL and ASL have a considerable effect on the overall cell volume expansion and stress behavior during redox cycling. Previous work [15] has shown that coarsely structured anode samples (with higher porosity) experience only a small volume change (<0.5%) upon re-oxidation, as determined by thermomechanical analysis. However, finer-grained samples (in a simulated AFL) increase in volume by 0.9–2.5% after re-oxidation [15], resulting in electrolyte cracking.

3.2. Characteristics of isothermal (800 °C) redox cycling

Isothermal redox cycling was carried out to determine the extent of damage to the Ni–YSZ supported samples caused by complete Ni oxidation after long times in air at constant temperature, for comparison with the non-isothermal data discussed below. The results, involving five full cycles (Fig. 2) of the Ni–YSZ anode-supported discs (Fig. 1) at 800 °C in the TGA, are shown in Fig. 4, revealing the mass gain (Fig. 4a) and loss (Fig. 4b) observed during exposure to air and H_2, respectively. In all cases, the mass is normalized with respect to the theoretical oxygen mass loss or gain,

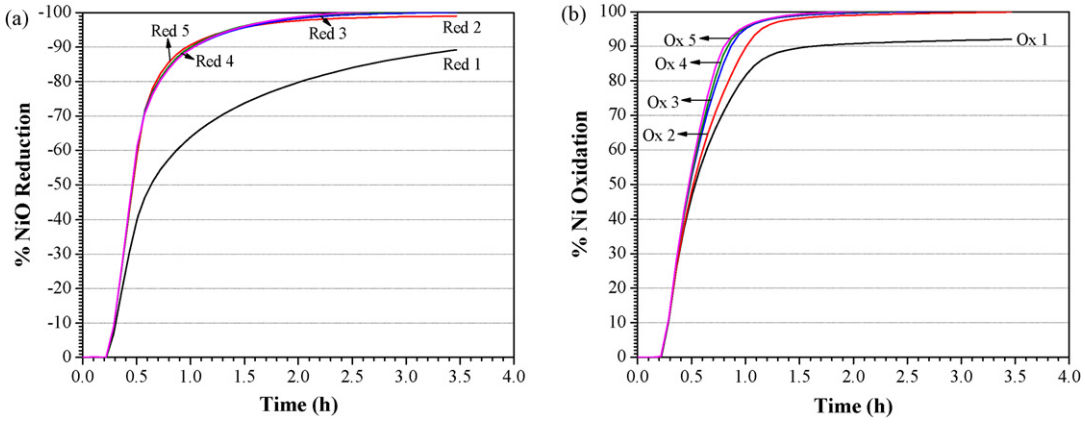

Fig. 4. Typical mass gain (a) and loss (b) TGA responses for Ni–YSZ/YSZ samples (Fig. 1) at constant temperatures of 800 °C, using the redox cycling protocol shown in Fig. 2.

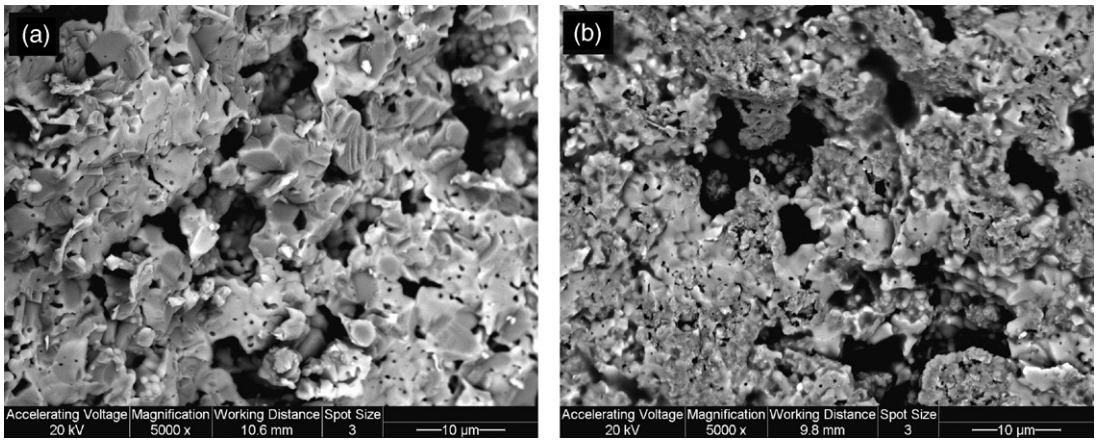

Fig. 5. Top-down SEM-BSE views of Ni–YSZ/YSZ samples (Fig. 1) in fully oxidized state (a) as sintered, and (b) after five redox cycles at 800 °C.

respectively, equivalent to 100% reduction or oxidation of the Ni component.

It is seen in Fig. 4a that the first reduction of the as-prepared NiO–YSZ layer, forming Ni–YSZ, requires significantly more time (~10% of the Ni remains oxidized, even after 3.5 h) at 800 °C, in comparison with the subsequent reduction steps. After the second reduction step, close to full reduction of NiO is achieved in only ~2 h. The faster reduction rate during Reductions 2–5 vs. Reduction 1 may be attributed to microstructural changes (Fig. 5) of the NiO [22] during Oxidation 1 (in comparison to the as-sintered sample), allowing better accessibility to H_2 and to the opening of micro-fissures, due to volume expansion after re-oxidation [23]. Due to the high porosity of the re-oxidized NiO (Fig. 5), it is presumed that the NiO particles throughout the anode layer become more easily accessible to hydrogen, thus being more rapidly reduced after the first redox cycle number [24]. A similar phenomenon was reported by Fouquet et al. [11], who showed that re-oxidized NiO particles are finer and more porous than in the as-sintered state. Microstructural changes after re-oxidation were also observed by Klemenso et al. [25] during *in situ* redox studies in an Environmental Scanning Electron Microscope.

The reduction plots (Fig. 4a) show an initial, short period of time (13 min) before the anode begins reducing; this includes the 10 min N_2 purge, a delay for N_2 to move out of the lines to be replaced with H_2, and a very short induction period (related to H_2 adsorption, H–H bond-breaking, and oxygen anion vacancy creation) until the first Ni grains are created on the surface [26]. Following this, the plot shows a linear mass loss at both temperatures, up to 65–70% reduction, and then a slower reduction rate thereafter. This change may indicate that the unreduced NiO regions are becoming more difficult to reach by H_2, partly due to the formation of a Ni blocking layer around the NiO particles, which would then inhibit the escape of water and hence decreases the reaction rate [15].

Fig. 4b shows that the first oxidation cycle also takes substantially more time than do the subsequent oxidation steps. Note that incomplete reduction in the first cycle in H_2 (Fig. 4a) makes it appear that not all of the Ni is oxidized in the first oxidation cycle (Fig. 4b), even though the sample has clearly stopped gaining mass. In fact, the anode has been 100% oxidized in all oxidation cycles at both testing temperatures after 2 h of air exposure.

From the oxidation TGA data, all in 20% O_2–He (Fig. 4b), a linearity in mass gain with time is seen up to ~ 50% Ni to NiO conversion and then a gradual decrease in the oxidation rate is noted (it takes 30 min to oxidize ~50%, 45 min to oxidize ~70%, and 1 h to oxidize ~90% of the Ni in the anode). Clearly, oxidation proceeds rapidly at bare metallic Ni particles and then slows down, likely in relation to slow cation transport through the thickening NiO layer [27]. The slower oxidation kinetics at longer times may also arise from the presence of a gradient in O_2 partial pressure through the depth of the anode, exacerbated by the blocking effect of the NiO formed near the anode/air surface, which further narrow the pores in this region [28].

Higher oxidation rates with increasing redox cycle number have been shown by Young et al. [29] to also correlate with the number and size of the cracks that develop in the electrolyte. It was proposed that this allows for better oxygen access into the anode, as the air can now penetrate from both the porous anode and the cracked electrolyte sides of the cell, thus decreasing gas transport limitations. However, there is still a slow-down seen in the rate of oxidation after 90% of the Ni is oxidized, even after the electrolyte cracks have formed.

After undergoing five full redox cycles, all at 800 °C, the anode-supported samples were examined using optical microscopy. Fig. 6 shows a top-down optical view of the electrolyte side of the samples, showing numerous cracks, as expected. This is consistent with the work of Malzbender et al. [22], who showed the damaging effect of multiple redox cycles on the microstructure (>60% volume expansion of the Ni component) of anode-supported planar Ni–YSZ half-cells. The major cause of the expansion upon oxidation

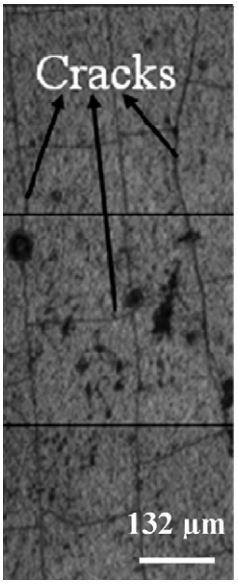

Fig. 6. Top-down optical microscopy view of cracks in YSZ electrolyte after five redox cycles (Fig. 2) of Ni–YSZ/YSZ sample (Fig. 1), all at 800 °C.

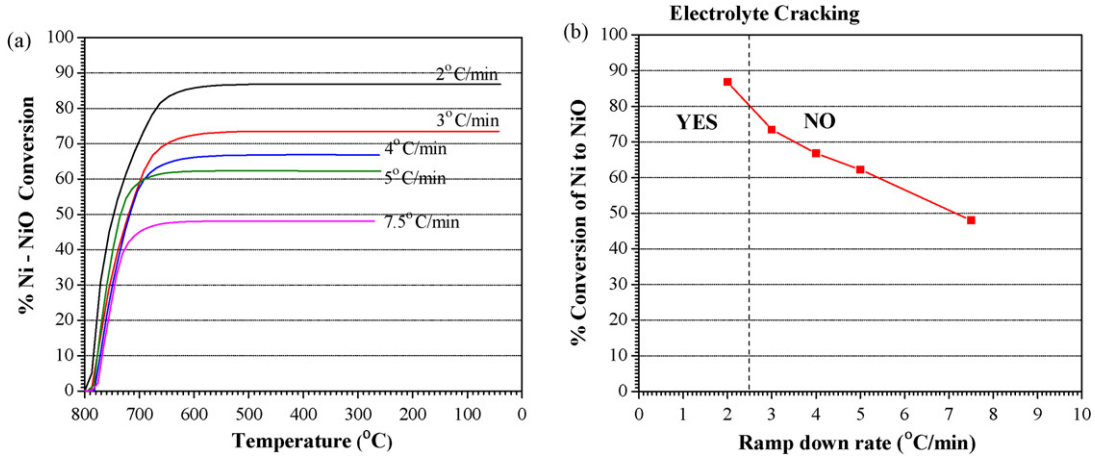

Fig. 7. Cool-down of Ni–YSZ/YSZ samples (Fig. 1) in air during TGA analysis at rates shown, all from a starting temperature of 800 °C: (a) % mass gain during Ni oxidation, and (b) % Ni to NiO conversion, in relation to observed cracks in the electrolyte, as a function of cell cool-down rate.

Table 1
Effect of cooling rate in air on extent of Ni–YSZ/YSZ sample oxidation.

Cool-down rate (°C min^{-1})	Time taken to cool to 250 °C (min)	% mass change (TGA)	Thickness of NiO film on Ni particles[a] (μm)
2	125	87	2.1
3	83	74	1.1
4	62	67	1.05
5	50	62	0.7
7.5	33	48	0.5

[a]Thickness of NiO film on Ni particles located 0.95 mm into Ni–YSZ anode support layer (Fig. 9), as determined from cross-sectional SEM images using ImageJ Software.

of the Ni–YSZ composite is the formation of closed porosity in the anode, leading to stress build-up [30]. The resulting tensile stresses cause mechanical degradation and cracking, leading to cell failure, although it is currently uncertain how much the changed NiO morphology (Fig. 5) contributes to the severity of the degradation.

3.3. Minimizing NiO formation by cell cool-down during air exposure

3.3.1. Optimization of cell cool-down rate

In the present work, the primary goal has been to prevent electrolyte cracking during air exposure. This was achieved by cooling the Ni–YSZ anode support layer (plus the thin YSZ electrolyte), in air, down to a temperature at which the rate of Ni oxidation would be sufficiently slowed down ('non-isothermal' redox cycling). The non-isothermal redox cycling experiments (Fig. 3) were carried out as follows. After 3.5 h at 800 °C in H_2 (followed by a 5 min N_2 purge), air (20% O_2–He) was allowed into the cell and the temperature was immediately decreased at various ramp-rates. TGA was used to measure the mass gain (Fig. 7) of the specimens as a result of Ni oxidation. When the temperature reached 250 °C and after a short N_2 purge, the temperature was increased again to 800 °C in H_2 at a ramp rate of 7.5 °C min^{-1}. The extent of Ni oxidation was determined at five different ramp-down rates from 2 to 7.5 °C min^{-1}. Each cool-down cycle was repeated nine times to ensure that any cumulative damage from sintering would also be captured.

It is seen in Fig. 7a that the rate of oxidation decreases significantly once the temperature during ramp-down reaches ~600 °C, consistent with the literature [16,17], which has shown that the rate of Ni oxide formation is very slow in this temperature range. For these samples, all cooled in air from 800 °C, Table 1 and Fig. 7 show that, the more rapid the cooling rate, the less Ni oxidation is seen. This makes sense, as the more quickly the temperature is lowered, there is less dwell time at temperatures (>600 °C) at which Ni oxidation is rapid. This is illustrated by the near-linear relationship between % oxidation and ramp-down rate (which is inversely proportional to the amount of time spent at >600 °C) seen in Fig. 7b.

Fig. 8a and b shows top-down optical micrographs of the YSZ electrolyte surface after nine non-isothermal redox cycles at 2 and 3 °C min^{-1}, respectively, all from 800 °C. As can be seen, the sample cooled at 2 °C min^{-1} shows severe cracking of the electrolyte, starting at the edges, and micro-cracking throughout the electrolyte layer, while no cracking is seen in the sample cooled at 3 °C min^{-1}. The dashed vertical line shown in Fig. 7b indicates the cooling

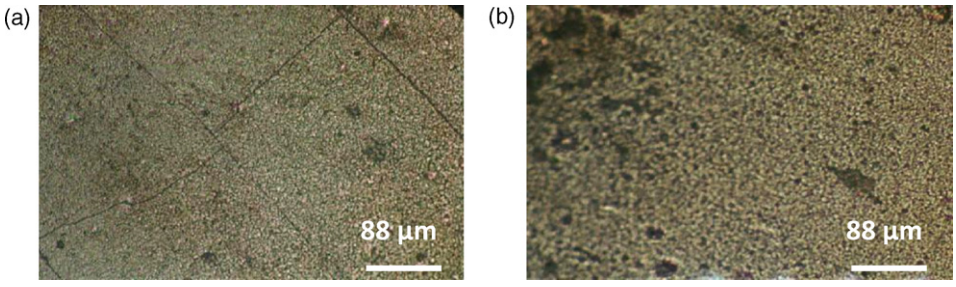

Fig. 8. Top-down optical microscopy views of the YSZ electrolyte for Ni–YSZ/YSZ sample (Fig. 1) in oxidized state at 800 °C after nine cool-down cycles at (a) 2 °C min^{-1} and (b) 3 °C min^{-1}. Cracking is seen in (a), but not in (b) or for cooling rates >3 °C min^{-1}.

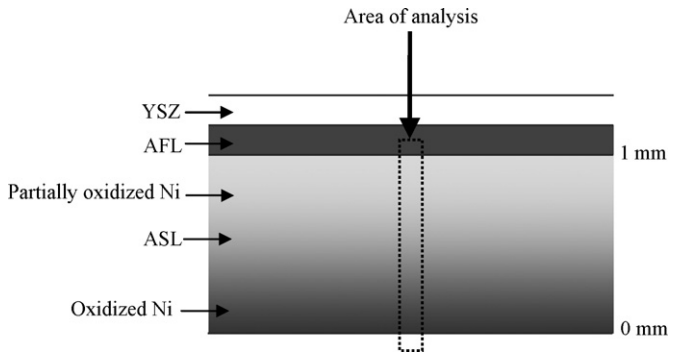

Fig. 9. Schematic illustration of half-cell cross-section, showing region of SEM analysis (dashed rectangle) used in Fig. 10 and also demonstrating the gradient in the oxidized Ni content within the anode support layer. The scale on the right indicates the depth into the anode, of relevance in Figs. 12 and 13.

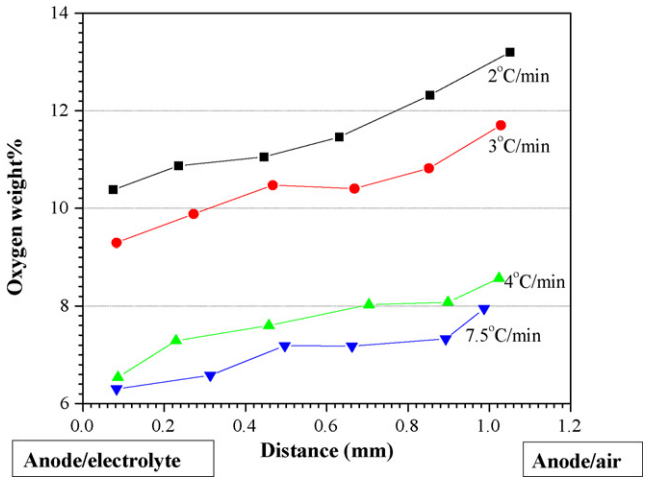

Fig. 11. EDX analysis of Ni–YSZ/YSZ sample (Fig. 1) at different depths into the ASL (0 mm is at air/ASL interface and 1 mm is at ASL/YSZ interface, as shown in Fig. 9), after nine cool-down cycles from 800 °C.

rates above and below which no cracking, vs. cracking, respectively, was seen in the optical images, such as shown in Fig. 8. It was expected that, as the cooling rate increased, thermal shock degradation would become a factor, but no damage was seen for samples cooled at between 3 and 7.5 °C min^{-1}. It is possible that, in stacks with larger-sized cells, cracks caused by thermal shock may result, and thus the cooling rate will need to be optimized for systems in practice.

3.3.2. *Microstructural analysis of Ni–YSZ anode layer as a function of cool-down rate*

To more fully understand the effect of cell cool-down in air on the anode microstructure and composition (Ni vs. NiO), an optical microscopy analysis of the anode support layer (ASL) was carried out in the region indicated in Fig. 9 (the dashed rectangle) to detect the areas that were predominantly oxidized (duller optically) vs. those that are still reduced (brighter, due to optically reflective metallic Ni). In this study, the Ni–YSZ anode support layers were subjected to nine non-isothermal redox cycles, as before, at different cooling rates.

Fig. 10a shows an image of a fully reduced (at 800 °C) Ni–YSZ anode sample (in the rectangular region shown in Fig. 9), while Fig. 10b–d shows the same region, but for samples that were cooled down in air at 7.5, 3 and 2 °C min^{-1}, respectively. Fig. 10e shows a fully oxidized Ni–YSZ specimen, formed isothermally at 800 °C in air, for comparison. As expected, the fully reduced sample in Fig. 10a has the largest density of bright (metallic Ni + YSZ) particles, while Fig. 10e is homogeneously much duller (NiO + YSZ).

For the sample cooled at 7.5 °C min^{-1} during exposure to air (Fig. 10b) from 800 °C, the sample is seen to have retained significant metallic content all the way to the outer anode/air interface (note that the TGA results in Fig. 7 show that this sample is close to 50% oxidized). In comparison, for samples that were cooled slowly at 3 and 2 °C min^{-1} (Fig. 10c and d, respectively), the outer region of the ASL seems to be fully oxidized, while the deeper regions of the anode are also heavily oxidized. Specifically, in Fig. 10d (sample cooled at 2 °C min^{-1}), the ASL appears to be more or less fully oxidized, consistent with the 87% NiO content, overall, obtained by TGA (Fig. 7). This sample (2 °C min^{-1}) showed electrolyte cracking (Fig. 8a), while the samples cooled at rates higher than 3 °C min^{-1} were crack-free.

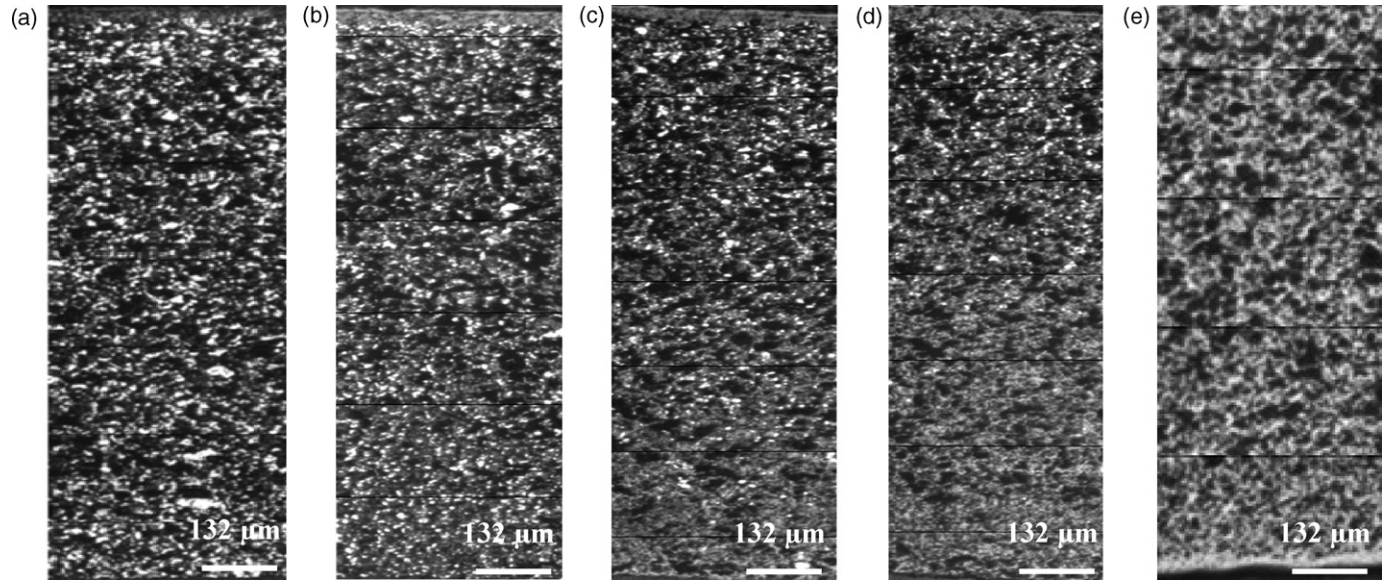

Fig. 10. Cross-sectional optical microscopy images of Ni–YSZ/YSZ samples in sequence of: (a) fully reduced to Ni at 800 °C, and after nine heating (to 800 °C)/cooling (to 250 °C) cycles at cooling rates of (b) 7.5 °C min^{-1}, (c) 3 °C min^{-1} and (d) 2 °C min^{-1}, and (e) as-sintered 100% NiO.

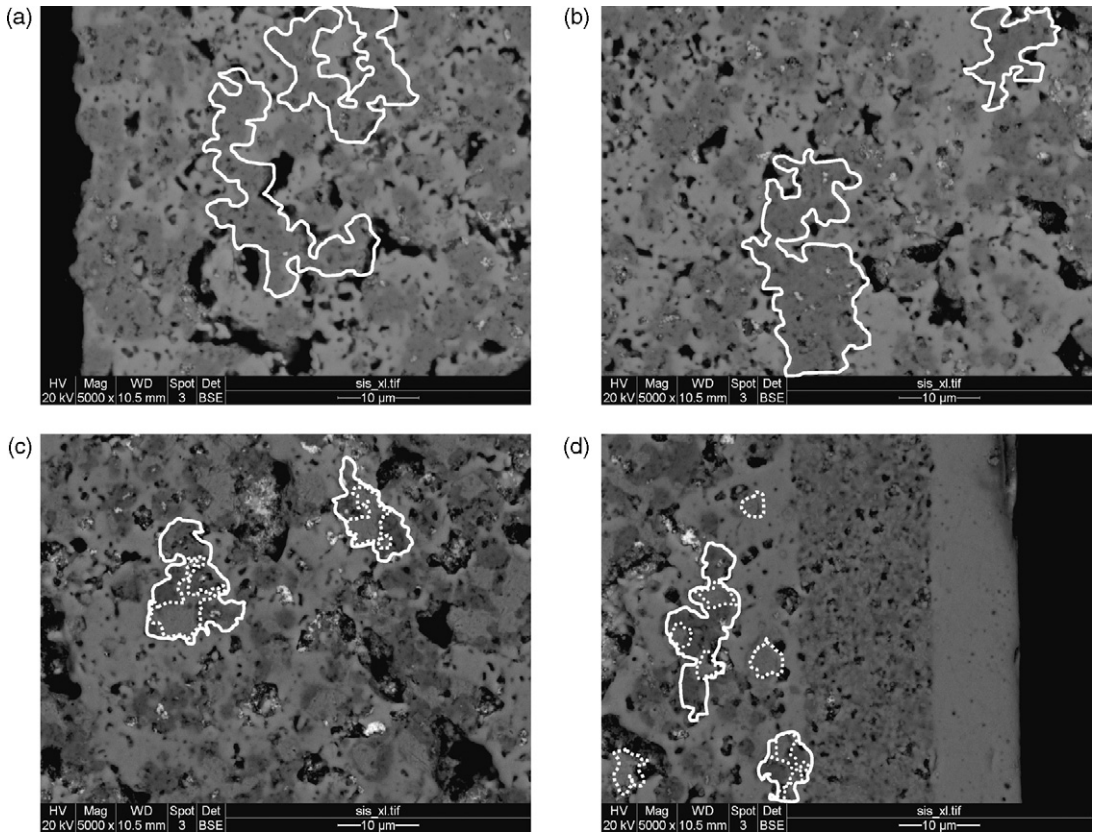

Fig. 12. SEM cross-sectional views of Ni–YSZ/YSZ samples (Fig. 1) after nine cool-down cycles, all from 800 °C at 2 °C min^{-1} at the following distances into the anode from the anode/air interface (a) 0.03 mm, (b) 0.31 mm, (c) 0.6 mm, and (d) 0.94 mm. The white dotted lines outline some of the Ni regions and the white solid lines encircle the NiO regions.

The gradient in oxygen content suggested in Fig. 10 was also confirmed using energy dispersive X-ray analysis (EDX) in the SEM, as presented in Fig. 11. These analyses were carried out throughout the cross-section of the anodes, but within the area represented by the 'rectangle' shown in Fig. 9. Although these results are again only qualitative (the oxygen content is much lower than the real values due to sample surface roughness), they do indicate clearly that the extent of Ni oxidation (the oxygen content) is higher in the outer, vs. inner, regions of the anode layer at all cooling rates. Also, Fig. 11 confirms that the slower cooling rates allow a higher extent of oxidation, overall, consistent with the longer times spent at high temperatures. Fig. 9 shows a schematic drawing of what is seen in Figs. 10 and 11, namely that there is a gradient in the NiO content within the ASL during cell cool-down in air, with the outer regions being more oxidized than those deeper in the anode and closer to the electrolyte.

To examine the oxygen gradient more closely, back-scattered SEM and EDX analysis of the 1 mm thick Ni–YSZ anode support layer was carried out. Figs. 12 and 13 show the ASL cross-sectional microstructures after nine heating (to 800 °C) and cool-down cycles (to 250 °C) at 2 and 7.5 °C min^{-1}, respectively, at various depths into the ASL (within the rectangular area shown in Fig. 9). NiO is darker than YSZ in the SEM images, but Ni and YSZ cannot be easily distinguished. For this reason, particles that are predominantly Ni or NiO (confirmed by EDX analysis) are outlined using dashed and solid lines, respectively, in Figs. 12 and 13.

At a slow cooling rate of 2 °C min^{-1}, Fig. 12a and b shows that, to a depth into the anode of 0.3 mm, essentially all of the Ni is oxidized, while Fig. 12c and d shows that many particles are partially oxidized. It is clear that the 2 °C min^{-1} cooling rate in air (Fig. 12d) allows enough time for most of the anode layer to oxidize (TGA data in Fig. 7a showed that 87% of the Ni is converted to NiO). At a cool-down rate of 7.5 °C min^{-1}, Fig. 13 shows that significantly less NiO is present at all depths, vs. in the 2 °C min^{-1} cooled sample (Fig. 12). This is consistent with the TGA data (Table 1), which show that only 48% of the total Ni content was oxidized during cell cool-down at 7.5 °C min^{-1} in air. Fig. 13 also shows that the particles in the outer regions of the anode support layer are only partly oxidized, while at depths >∼0.7 mm, almost no NiO is seen.

The average thickness of the NiO film on the surface of the Ni particles located at ∼0.95 mm from the ASL/air interface (Fig. 9), very close to the AFL and thin electrolyte layer, was then measured. Table 1 and Fig. 14 show that the oxide thickness decreases with more rapid cool-down in air. It is also seen in Table 1 that, when the NiO film on the Ni particle surface is greater than ∼1 μm in thickness in the region near the electrolyte, which is seen for cooling rates <3 °C min^{-1}, the stress developed was sufficient to cause the electrolyte to crack (Fig. 8a). Using the average particle size and the Ni and NiO densities, a 1 μm oxide film thickness was calculated to be equivalent to ca. 80% oxidation of the Ni particles in this region (cf. with the 87% overall extent of oxidation of this sample, as determined from TGA). For conditions under which electrolyte cracking was not seen, the NiO film thickness on Ni particles located close to the electrolyte is 0.75 μm (or smaller), which can be translated to 65% oxidation (or less).

The low oxygen content near the electrolyte helps to explain why anodes that are cooled down at rates >3 °C min^{-1} do not exhibit electrolyte cracking. This is the result of the consumption of oxygen in the outer region of the anode layer during NiO formation, thus substantially lowering the pO_2 deeper in the anode, which in turn, lowers the rate of Ni oxidation in this region. Also, the NiO particles formed in the outer regions of the anode are larger (by 65% [8]) than

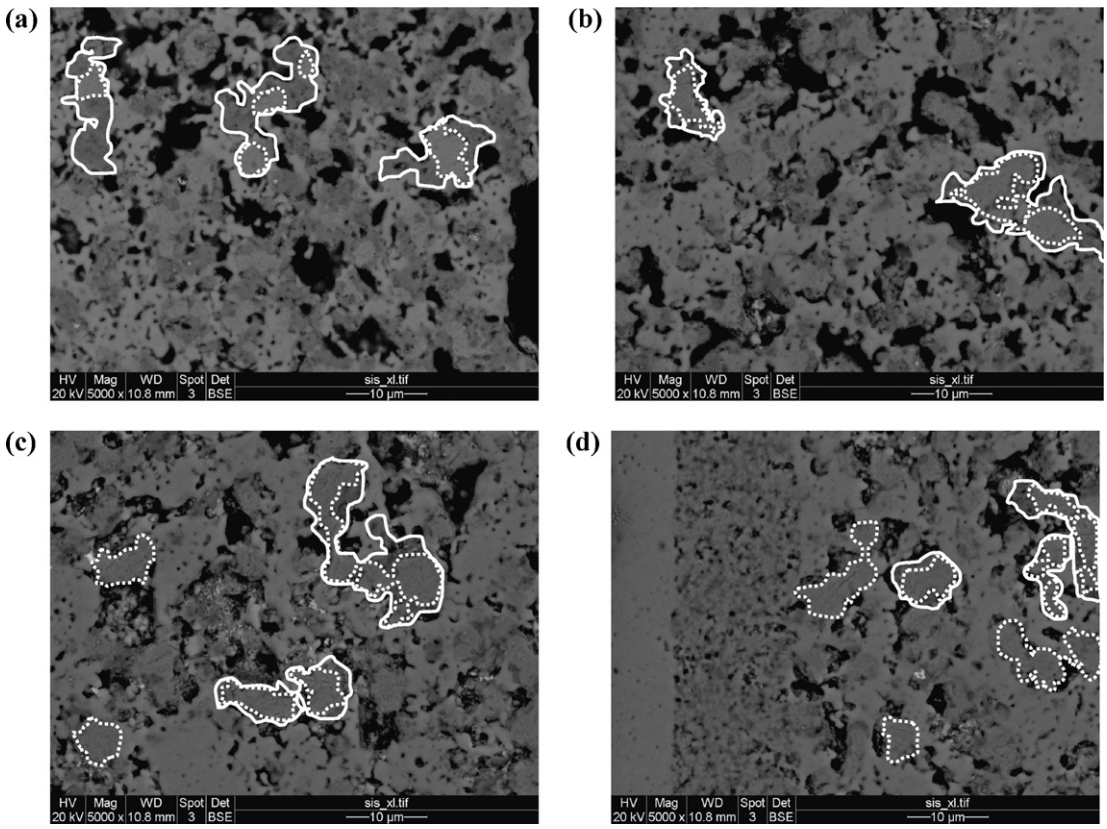

Fig. 13. SEM cross-sectional views of Ni–YSZ/YSZ samples (Fig. 1) after nine cool-down cycles from 800 °C, all at 7.5 °C min^{-1} in air, at the following distances into the anode from the anode/air interface: (a) 0.04 mm, (b) 0.43 mm, (c) 0.69 mm, and (d) 0.96 mm. The white dotted lines outline some of the Ni regions and the white solid lines encircle the NiO regions.

the original Ni particles, thus lowering the porosity in the outer regions of the ASL (from ~38% and approaching ~22%). The smaller pores at the anode/air interface will result in diminished access to O_2, thus delaying access to the inner regions of the anode.

At faster cool-down rates, this is not as much of an issue since the Ni does not fully oxidize in any part of the cell. Under these conditions, by the time any un-reacted oxygen reaches the inner regions of the anode, the temperature should be low enough such that the rate of Ni oxidation is also very low. Overall, these results show that, if the extent of oxidation of the Ni particles situated deep within the anode layer can be maintained at less than 65%, this produces tolerable stresses on the adjacent electrolyte layer and no cracking ensues.

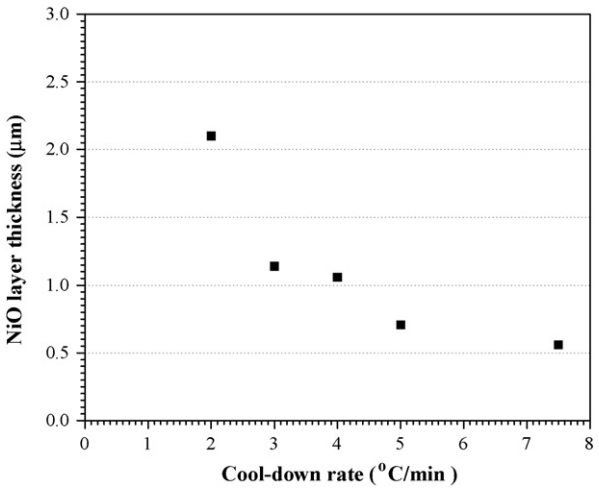

Fig. 14. Thickness of NiO, measured using ImageJ Software, surrounding Ni particles in the region near the electrolyte (0.95 mm into ASL, Fig. 9), formed during cool-down at various rates in air, all starting from 800 °C.

The fact that Ni oxidation is anisotropic within the anode layer also argues that the TGA oxidation data, in general, cannot be interpreted using conventional oxide growth kinetic laws, which assume that all of the Ni surface sites are in an identical environment at all times. In fact, Ni particles deeper in the anode support are covered with a thinner oxide layer than particles closer to the outer surface (as seen in Figs. 12 and 13) and thus will be oxidizing at different rates. Furthermore, the O_2 partial pressure (pO_2) will vary within the ASL, with a higher pO_2 in the outer vs. inner regions of the ASL. This may help to explain why the TGA data obtained for porous Ni–YSZ anode layers, examined both here and in the literature [31], do not generally obey classical growth laws for Ni metal in air [29,32].

4. Summary

The primary goal of this work has been to develop a possible method to minimize the mechanical degradation of Ni–YSZ anode-supported SOFCs caused by redox cycling at high temperatures in air. Isothermal TGA experiments indicate that the rate of Ni oxidation is initially linear up to ~50% conversion and then decreases. Diffusion limitations of air through the newly formed NiO layer are likely the cause of this deviation from linearity, but the pores of the ASL layer itself are also closing off and will further limit gas transport. The increasing rate of oxidation with repeated redox cycling is primarily due to air leakage through an increasingly micro-cracked YSZ electrolyte, thus easing these gas transport limitations.

Non-isothermal TGA analysis shows that, the faster the cooling rate, the lower the mass gain due to NiO formation, with the over-

all extent of oxidation being 85–90% at 2 °C min^{-1} and close to 50% at 7.5 °C min^{-1}. The samples show mechanical damage (cracking) when cooled at <3 °C min^{-1}, whereas at ≥3 °C min^{-1}, no cracks are seen in the sample. For these partially oxidized anode layers, optical microscopy and oxygen EDX analysis both show that the Ni located in the outer regions of the Ni–YSZ layer is substantially more oxidized than are the Ni particles closer to the electrolyte layer, at all cooling rates investigated. This is likely the reason that cell cooling is successful in preventing electrolyte cracking during a redox cycle.

Overall, it is concluded that anode-supported cell damage can be avoided by cooling the cell during air exposure. Although no damage from thermal shock during cooling, even at 7.5 °C min^{-1}, was observed, this may be due to the small sample size. Thus, the cooling rate should be rapid enough to ensure that the Ni particles deep in the anode layer (near the AFL and the electrolyte) are not fully oxidized (3 °C min^{-1}), while also being sufficiently slow such that thermal shock is not an issue. It should also be noted that the approach developed here to prevent cell cracking during redox cycling may only be valid for cells containing thick anode layers (1.1 mm) and thus more work is needed to determine the minimum anode thickness for which this method will prevent cell failure. Also, the maximum cooling rate will be dictated by the cell and stack design and thus this also needs further investigation.

Acknowledgements

We gratefully acknowledge the financial support of the Natural Sciences and Engineering Research Council of Canada (NSERC), through the Strategic Research Project and Strategic Research Network (Solid Oxide Fuel Cells Canada) granting programs, as well as the Canada Foundation for Innovation (CFI) and the Alberta Science and Research Authority for infrastructure support.

References

[1] C.S. Song, Catalysis Today 77 (2002) 17–49.
[2] A. Atkinson, S. Barnett, R.J. Gorte, J.T.S. Irvine, A.J. Mcevoy, M. Mogensen, S.C. Singhal, J. Vohs, Nature Materials 3 (2004) 17–27.
[3] S. Majumdar, T.D. Claar, B.K. Flandermeyer, Journal of the American Ceramic Society 69 (1986) 628.
[4] T.W. Eom, H.K. Yang, K.H. Kim, H.H. Yoon, J.S. Kim, S.J. Park, Ultramicroscopy 108 (2008) 1283–1287.
[5] S. DeSouza, S.J. Visco, L.C. DeJonghe, Solid State Ionics 98 (1997) 57–61.
[6] C.R. Xia, M.L. Liu, Solid State Ionics 144 (2001) 249–255.
[7] S.M. Haile, Acta Materialia 51 (2003) 5981–6000.
[8] D. Sarantaridis, A. Atkinson, Fuel Cells 7 (2007) 246–258.
[9] M. Cassidy, G. Lindsay, K. Kendall, Journal of Power Sources 61 (1996) 189–192.
[10] D. Waldbillig, A. Wood, D.G. Ivey, Journal of Power Sources 145 (2005) 206–215.
[11] D. Fouquet, A.C. Muller, A. Weber, E. Ivers-Tiffee, Ionics 9 (2003) 103–108.
[12] A. Wood, M. Pastula, D. Waldbillig, D.G. Ivey, Journal of the Electrochemical Society 153 (2006) A1929–A1934.
[13] Q.X. Fu, F. Tietz, D. Sebold, S.W. Tao, J.T.S. Irvine, Journal of Power Sources 171 (2007) 663–669.
[14] S.W. Tao, J.T.S. Irvine, Nature Materials 2 (2003) 320–323.
[15] D. Waldbillig, A. Wood, D.G. Ivey, Solid State Ionics 176 (2005) 847–859.
[16] B. Liu, Y. Zhang, B.F. Tu, Y.L. Dong, M.J. Cheng, Journal of Power Sources 165 (2007) 114–119.
[17] R. Peraldi, D. Monceau, B. Pieraggi, Oxidation of Metals 58 (2002) 275–295.
[18] J. L. Young, V. Vedahara, S. Kung, S. Xia, V. I. Birss, 2007. ECS Transactions (ECST, Vol.7, Issue 1), 10th International Symposium on Solid Oxide Fuel Cells (SOFC-X), June 3–8, 2007, Nara, Japan.
[19] D. Waldbillig, A. Wood, D.G. Ivey, Journal of the Electrochemical Society 154 (2007) B133–B138.
[20] Y. Zhang, B. Liu, B.F. Tu, Y.L. Dong, M.J. Cheng, Solid State Ionics 176 (2005) 2193–2199.
[21] S.P. Jiang, Y.Y. Duan, J.G. Love, Journal of the Electrochemical Society 149 (2002) A1175–1183.
[22] J. Malzbender, E. Wessel, R.W. Steinbrech, Solid State Ionics 176 (2005) 2201–2203.
[23] S. Modena, S. Ceschini, A. Tomasi, D. Montinaro, V.M. Sglavo, Journal of Fuel Cell Science and Technology 3 (2006) 487–491.
[24] T. Klemenso, C. Chung, P.H. Larsen, M. Mogensen, Journal of the Electrochemical Society 152 (2005) A2186–A2192.
[25] T. Klemenso, C.C. Appel, M. Mogensen, Electrochemical and Solid-State Letters 9 (2006) A403–A407.
[26] J.T. Richardson, R. Scates, M.V. Twigg, Applied Catalysis A: General 246 (2003) 137–150.
[27] M. Pihlatie, A. Kaiser, M. Mogensen, Solid State Ionics 180 (17–19) (2009) 1100–1112.
[28] N.M. Tikekar, T.J. Armstrong, A.V. Virkar, Journal of the Electrochemical Society 153 (4) (2006) A654–A663.
[29] J.L. Young, V. Vedahara, S. Kung, S. Xia, V.I. Birss, ECS Transactions (ECST 7(1)) 10th International Symposium on Solid Oxide Fuel Cells (SOFC-X), 2007.
[30] D. Sarantaridis, R.J. Chater, A. Atkinson, Journal of the Electrochemical Society 155 (5) (2008) B467–B472.
[31] G. Stathis, D. Simwonis, F. Tietz, A. Moropoulou, A. Naoumides, Journal of Materials Research 17 (2002) 951–958.
[32] V. Vedharathinam, M.Sc. Thesis, University of Calgary, Calgary, Canada (2009).